Scientia Iranica, Vol. 11, Nos. 1&2, pp 128–137

SCIENTIA IRANICA

Research Note

A Numerical Comparison of 2-D Inviscid and Viscous Approaches for Flow Through a Stage of an Axial Compressor

B. Farhanieh*, N. Amanifard[1] and K. Ghorbanian[2]

In this paper, an unsteady, two-dimensional solver is developed, based on Van Leer's flux splitting algorithm, in conjunction with the "Monotonic Upstream Scheme for Conservation Laws (MUSCL)" limiters for improving the order of accuracy. For a minimum usage of computer memory and faster convergence, the two-layer Baldwin-Lomax turbulence model is implemented for a viscous solution. Three test cases are prepared to validate the solver. The computed results are compared with experimental data and the good agreement of the compared results validates the solver. Finally, the solver is used for the flow through a multi-blade stage of an axial compressor in its design condition. The solutions of inviscid and viscous flows are prepared and the computed results are compared with each other, to show the accuracy of an inviscid approach, with respect to the viscous flow at the design operating point. The comparison shows that the viscous approach is more acceptable.

INTRODUCTION

Historically, analysis of the flow field in the close vicinity of the stability limit and the design point, especially in Gas-Turbine engines, has been based mainly on experimental observations and studies. Recently, several Computational Fluid Dynamics (CFD) codes have been developed to give more powerful, low-cost design tools. Axial compressors, with their adverse pressure gradients in a through flow direction, are the most critical component in gas-turbine engines from the viewpoint of flow instability phenomena. Today, the use of CFD tools is a standard practice in the study of the cascade flow within the stable operating range of a compressor, but the CFD approach still needs to be established as a sound prediction method for operation in the unstable region. Notable progress in the use of CFD-type techniques for the calculation of instability effects has been made by Sisto et al. [1] and Jonnavithula et al. [2]. They used a two-dimensional discrete vortex model with the separation point being obtained by an integral boundary layer. The evolution of stall is well predicted when compared with their experiment, although only up to six blade passages are used in the computation. Further, a numerical study was made by He [3] in a single stage of an axial compressor. The Navier-Stokes equations were discretized in space by the finite volume method and integrated in time by using a four stage Rung-Kutta scheme. Second- and fourth-order blended smoothing was adopted in both the streamwise and circumferential directions for numerical damping and the Baldwin-Lomax turbulence model was also adopted. Outa et al. [4] made a numerical simulation for stall cells in the rotor-stator frame of a compressor, using a viscous approach. Furthermore, a numerical study was made by Saxer et al. [5] for an inviscid flow passing through axial compressors and the history of stall vortices were investigated for a fifteen-blade passage of a single stage. The mass flow rate fluctuations were approximately similar to those obtained from experimental observations.

Observing the studies mentioned above, it would seem useful to demonstrate the differences between the viscous and inviscid approaches, before any investigation about flow instabilities through a stage of an axial compressor.

The scope of this work is twofold. First, to

*. *Corresponding Author, Department of Mechanical Engineering, Sharif University of Technology, Tehran, I.R. Iran.*

1. *Department of Mechanical Engineering, Guilan University, Rasht, I.R. Iran.*
2. *Department of Aerospace Engineering, Sharif University of Technology, Tehran, I.R. Iran.*

introduce and validate a two-d1imensional, density-based, flow equations solver and, second, to prepare numerical comparison of using viscous and inviscid approaches in compressor studies, before using them in instability conditions.

In the present work, computational test cases have been carried out to validate the solver and to study the implementation of flux splitting methods with MUSCL limiters in a multi-block computational domain. The modified Baldwin-Lomax model is used for the viscous solutions.

GOVERNING EQUATIONS

For a given thermodynamic system having two intensive degrees of freedom, its fluid dynamic behavior can, generally, be described by means of the system of conservation laws corresponding to the conservation of total mass, momentum and energy.

Let $\mathbf{Q}$ be an unknown vector, defined for a two-dimensional study, as follows:

$$\mathbf{Q} = [\rho, \rho u, \rho v, \rho E]^T = [q_1, q_2, q_3, q_4]^T, \tag{1}$$

where E is the total energy ($E = e + (u^2 + v^2)/2$).

The equation of motion in its differential form is as follows:

$$\frac{\partial}{\partial t}\mathbf{Q} = -\nabla.\vec{\mathbf{F}}. \tag{2}$$

This accounts for the inviscid ($\vec{\mathbf{F}}_E$) and viscous ($\vec{\mathbf{F}}_v$) contributions, i.e.:

$$\vec{\mathbf{F}} = \vec{\mathbf{F}}_E - \vec{\mathbf{F}}_v, \tag{3}$$

where:

$$\vec{\mathbf{F}}_E = [\rho\mathbf{u}, \rho\mathbf{u}\mathbf{u} + p\mathbf{I}, \rho\mathbf{u}(E + P/\rho)]^T, \tag{4}$$

$$\vec{\mathbf{F}}_v = [0, \sigma, -(\mathbf{q} - \mathbf{u}.\ \sigma)]^T, \tag{5}$$

and:

$$\sigma = \mu(\nabla\mathbf{u} + \nabla\mathbf{u}^T) - \frac{2}{3}\mu\nabla.\mathbf{u}\mathbf{I}, \tag{6}$$

$$\mathbf{q} = -\lambda\nabla T. \tag{7}$$

The governing equations are transformed into a computaional space and the flux tensors are decomposed into two flux vectors $\overline{\mathbf{E}}$ and $\overline{\mathbf{F}}$. Hence, Equation 2 has the following general form:

$$\frac{\partial\overline{\mathbf{Q}}}{\partial\tau} + \frac{\partial\overline{\mathbf{E}_E}}{\partial\xi} + \frac{\partial\overline{\mathbf{F}_E}}{\partial\eta} = \frac{\partial\overline{\mathbf{E}}_v}{\partial\xi} + \frac{\partial\overline{\mathbf{F}}_v}{\partial\eta}. \tag{8}$$

Since the relative stagnation enthalpy is constant in the rotor (moving) frame, the governing equations for the relative frame are the same as those in the absolute frame, because there is no Coriolis acceleration (no radial component of velocity) and the only treatment in the stator (stationary) frame is the use of absolute velocity vectors in the place of relative velocities in the rotor (moving) frame. Quite obviously, the absolute velocities are achieved by adding the rotation speed to relative velocities.

NUMERICAL PROCEDURE

Cartesian Finite-Volume Method

Reconsidering Equation 8, the time derivative is approximated by a first-order backward differencing quotient and the remaining terms are written at time level $n+1$. Thus;

$$\frac{\overline{\mathbf{Q}}^{n+1} - \overline{\mathbf{Q}}^n}{\Delta\tau} + (\frac{\partial\overline{\mathbf{E}}}{\partial\xi})^{n+1} + (\frac{\partial\overline{\mathbf{F}}}{\partial\eta})^{n+1} = (\frac{\partial\overline{\mathbf{E}_v}}{\partial\xi})^{n+1} + (\frac{\partial\overline{\mathbf{F}_v}}{\partial\eta})^{n+1}. \tag{9}$$

Integrating Equation 9 over square ABCD, shown in Figure 1, and using Green's theorem provides:

$$\Delta\overline{\mathbf{Q}} + \frac{\Delta\tau}{\Delta\xi}(\overline{\mathbf{E}}_{Er} - \overline{\mathbf{E}}_{El}) + \frac{\Delta\tau}{\Delta\eta}(\overline{\mathbf{F}}_{Et} - \overline{\mathbf{F}}_{Eb}) = \frac{\Delta\tau}{\Delta\xi}(\overline{\mathbf{E}}_{vr} - \overline{\mathbf{E}}_{vl}) + \frac{\Delta\tau}{\Delta\eta}(\overline{\mathbf{F}}_{vt} - \overline{\mathbf{F}}_{vb}). \tag{10}$$

Since, in Equation 10, the flux vectors are evaluated in time step $n+1$, to evaluate them in time step n for an explicit solution, they can be expressed in terms of $\Delta\overline{\mathbf{Q}}$, by using the Taylor expansion and a first order

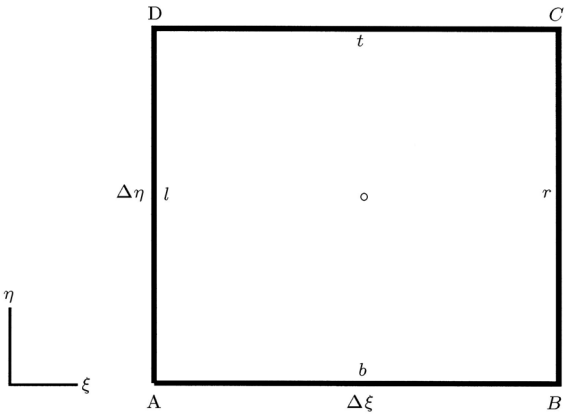

Figure 1. Definition of a finite-volume cell.

approximation in time, as follows [6]:

$$\overline{\mathbf{E}}^{n+1} = \overline{\mathbf{E}}^{n} + \frac{\partial \overline{\mathbf{E}}}{\partial \overline{\mathbf{Q}}} \Delta \overline{\mathbf{Q}} = \overline{\mathbf{E}}^{n} + \mathbf{A} \Delta \overline{\mathbf{Q}}, \tag{11a}$$

$$\overline{\mathbf{F}}^{n+1} = \overline{\mathbf{F}}^{n} + \frac{\partial \overline{\mathbf{F}}}{\partial \overline{\mathbf{Q}}} \Delta \overline{\mathbf{Q}} = \overline{\mathbf{F}}^{n} + \mathbf{B} \Delta \overline{\mathbf{Q}}, \tag{11b}$$

$$\overline{\mathbf{E}}_v^{n+1} = \overline{\mathbf{E}}_v^{n} + \frac{\partial \overline{\mathbf{E}_v}}{\partial \overline{\mathbf{Q}}} \Delta \overline{\mathbf{Q}} = \overline{\mathbf{E}_v}^{n} + \mathbf{A}_v \Delta \overline{\mathbf{Q}}, \tag{11c}$$

$$\overline{\mathbf{F}}_v^{n+1} = \overline{\mathbf{F}}_v^{n} + \frac{\partial \overline{\mathbf{F}_v}}{\partial \overline{\mathbf{Q}}} \Delta \overline{\mathbf{Q}} = \overline{\mathbf{F}_v}^{n} + \mathbf{B}_v \Delta \overline{\mathbf{Q}}. \tag{11d}$$

The matrices $\mathbf{A}, \mathbf{B}, \mathbf{A}_v,$ and $\mathbf{B}_v$ are Jacobian matrices and are computed in time n and Equation 10 is rearranged for $\overline{\mathbf{Q}}^{n+1}$, with respect to other terms evaluated in time step n.

Since evaluation of inviscid flux vectors on cell faces is the most important problem in the numerical solution of Euler and N-S equations, flux splitting methods are discussed in the following section.

The second-order derivatives are evaluated by central difference approximation.

Van Leer's Flux Vector Splitting Method

To avoid the addition of artificial viscosity and damping terms, flux vector splitting schemes are used to formulate the convective terms. The Van-Leer's flux splitting method is used in the present work.

In this method, the split fluxes are represented by a polynomial in $\mathbf{M}$ that gives the same functional values and slope of the unsplit fluxes at $\mathbf{M} = \pm 1$. Moreover, the symmetry properties of each split flux component should be the same as those of the unsplit one.

An extension of the Van Leer-type splitting to multidimensional flows is not quite trivial. The split flux component can be constructed by retaining the one-dimensional structure. Method conditions and the matrix form of split flux vectors for two dimensional studies in computational space is reported by Hoffman [6].

Construction of High-Order Methods

High-order methods can be constructed in many ways. Total Variation Diminishing (TVD) and the Monotonic Upstream Schemes for Conservation Laws (MUSCL) are the most famous methods related to the design of high-order schemes [7].

According to Van Leer's point of view, upwind methods can be interpreted as a projection phase followed by an evolution phase. In the projection (or reconstruction) phase, the piecewise continuous initial values are interpolated to yield a continuous distribution within each computational cell, while the evolution phase corresponds to the updating of an averaged unknown variable, $\widehat{u}$, exploiting the reconstructed solution.

In this work, the MUSCL limiter is used due to its high accuracy. For an unknown variable, u, the MUSCL can be expressed as [8]:

$$u_l^n = u_i^n + \frac{1}{4}\left[(1-r)\overline{\delta}^{+} u_{i-1}^n + (1+r)\hat{\delta}^{+} u_i^n\right], \tag{12a}$$

$$u_r^n = u_{i+1}^n - \frac{1}{4}\left[(1-r)\overline{\delta}^{+} u_{i+1}^n + (1+r)\hat{\delta}^{+} u_i^n\right]. \tag{12b}$$

A set of limiters are defined in Table 1 upon values of r. $\hat{\delta}^{+}$ and $\overline{\delta}^{+}$ are the limited slopes:

$$\hat{\delta}^{+} u = \ell(\delta^{+} u_i, \omega \delta^{+} u_{i-1}),$$

$$\overline{\delta}^{+} u = \ell(\delta^{+} u_i, \omega \delta^{+} u_{i+1}), \tag{13}$$

where $1 \leq \omega \geq (3-r)/(1-r)$ and ℓ is a limiter function, such as Van Leer and Roe's minmod limiter functions. The simplified form of MUSCL, using Van Leer's function, becomes [7]:

$$\ell = \frac{2\delta^{-} u . \delta^{+} u}{[(\delta^{-} u)^2 + (\delta^{+} u)^2]},$$

$$f = (1 - r \cdot \ell)\delta^{-} u + (1 + r \cdot \ell)\delta^{+} u,$$

$$u_r = u_{i+1,j} - \frac{1}{4} f \cdot \ell. \tag{14}$$

For the present work, the third order limiter ($r = 1/3$) is used.

As a result, the Van-Leer's flux splitting method decomposes the momentum fluxes in the above mentioned manner. To evaluate each decomposed flux on the cell faces, the limiter is implemented to increase the accuracy in a manner which minimizes the error growth. As reported by Farhanieh et al. [9], the Van-Leer's 3rd order limiter provides more accurate results with a relatively faster convergence history in time marching problems, with respect to other general limiters.

Table 1. Definition of limiters upon values of r.

r	Name of Limiter
1/3	Third-order upwind biased scheme
1	Three-point central difference scheme
-1	Fully upwind scheme
0	Fromm scheme

Stability Criteria

To overcome the solution instabilities in explicit techniques, the MacCormack stability criteria is employed to obtain the appropriate time step [6].

Numerical Boundary Conditions

Inflow and Outflow Boundary Conditions

For subsonic inflows, the three required variables from the upstream are the P_t, T_t and the inflow angle.

For subsonic outflows, the only required variable from the downstream is the set P_s. The other variables are determined from the computational domain by extrapolation.

Solid Wall Boundary Condition

For viscous solutions, the no-slip condition is implemented and, for inviscid cases, the free slip condition is used.

Initial Guess

Due to the hyperbolic-parabolic nature of the N-S equations in time marching methods, only one set of initial conditions is required. Pressure and temperature are set equal to total thermodynamics conditions of inflow and the velocity components are set equal to zero. These conditions are also implemented for the inviscid solutions.

Periodic Boundary Condition

For the upper and lower boundaries of the computational area of the rotor and stator frame, the periodic boundary condition is used to give the circumferential continuity of the cascades.

Neighborhood Block Boundary Condition

Each block shares one or more boundaries with its surrounding blocks. The exchange of data among the blocks takes place through their common boundaries.

At each time step, the solver sweeps all cells from the first to final block in turn. In this regard, the cell index is defined as follows:

$$ind(i,j) = i + [(iblock - 1)j\max - (j-1)]i\max. \tag{15}$$

Figure 2 shows the schematic shape of a computational domain near the common boundary of two adjacent blocks. In the overlap area, the fictitious cells of the upper and lower blocks cover each other. These cells do not exist physically and are just temporary cells to save boundary data. The fictitious cells of the upper block receive their information from the final inner cells of the lower block and the fictitious cells of the lower block receive their information from the first inner cells of the upper block. This extrapolation procedure is a first order approximation technique, which is a very common approximation in boundary cells in the computational domain.

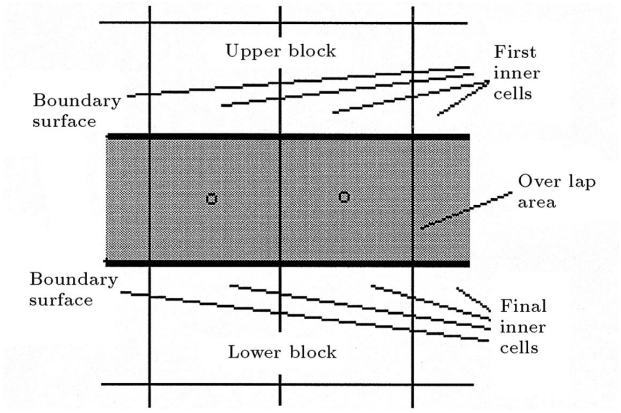

Figure 2. Schematic shape of block boundary condition.

Interface Boundary Condition

The interface boundary condition relates to the interchanging of flow information in the fictitious cells of the rotor and stator frames, which are located adjacent to the interface boundary. The mechanism of the interchanging of the information is very similar to that which is mentioned in the neighborhood block boundary condition section. The main difference is the adding of linear rotation speed to the vertical component of velocity coming from the rotor to stator blocks, in order to switch the solution to its absolute frame operation. However, the adverse mechanism is used to transfer the flow information from the stator to the rotor blocks. A nice advantage of using the upwind technique upon the flow characteristics, is that by receiving information into fictitious cells, it helps the solver prevent the growing of undesired errors in the computational domain.

Grid Generation

Each passage (between two blades) has an individual mesh, which is generated by a mesh generator program using the Partial Differential Equations (PDE) method. Clustering is available by related source terms, as well as orthogonality. The mesh generated for each individual passage is considered as a single block and the solver assembles them to prepare the complete area of solution by using the multi-block boundary condition. For a uniform basis, the mesh resolution used for both inviscid and viscous test cases is identical. The grid dependency behavior of the solver is studied

for airfoil studies in the following sections. The cells used for the stage problem have, relatively, the same aspect ratio of those in the airfoil problem. Also, a similar mesh resolution is used by Saxer et al. [5] in a multi-blade stage problem. As a result, the mesh resolution seems to be adequate for this work.

Turbulence Modeling

One of the groups of statistical turbulence models is the algebraic one- or two-layer turbulence closure. These models can easily be implemented into a numerical algorithm, but they require the determination of boundary layer parameters to calculate eddy viscosity. In complex flow, such as the flow through a turbine or compressor cascade, the calculation of, e.g., shear layer thickness in a CFD code is difficult, because no realistic criterion can be used to define the edge of the boundary layer [6]. That is, especially, the case when flow separation exists within the domain.

An algebraic model, which is not written in terms of the boundary layer quantities and is very robust in separated regions, is the modified Baldwin-Lomax (BL) model [6]. The BL model is implemented by He [3] in the numerical investigation of a Rotating-Stall inception in a multi-blade cascade flow in an axial compressor, where the flow may have large scale separated zones. Moreover, the comparison of other turbulence models, such as $\kappa - \epsilon$ with the BL model in [8], shows the adequate assurance of using the BL model in cascade problems. Regarding the large amount of memory required in multi-blade studies, the BL consumes the least memory and CPU time with respect to higher-order turbulence models. Consequently, for the present work, the BL model is preferred.

DISCUSSION OF RESULTS

Code Validations

The performance of the described methodology is assessed by comparing the computed results to other approved data.

The first validation test case is prepared for an inviscid flow over half of the NACA0012 airfoil. In Figure 3, the Pressure Coefficient (Cp) distribution was compared with results obtained by Hirsh [10]. The inlet Mach number is equal to 0.85 and the angle of attack is zero. The computed results are in good agreement with the reference data. This test case is prepared to validate the inviscid flow solution of the solver and its shock capturing capability.

The second test case is prepared for flow over a flat plate in the incompressible range of the Mach number ($\mathbf{M} = 0.2$). The Reynolds number is 10^6 and the transition point is set at the leading edge of the

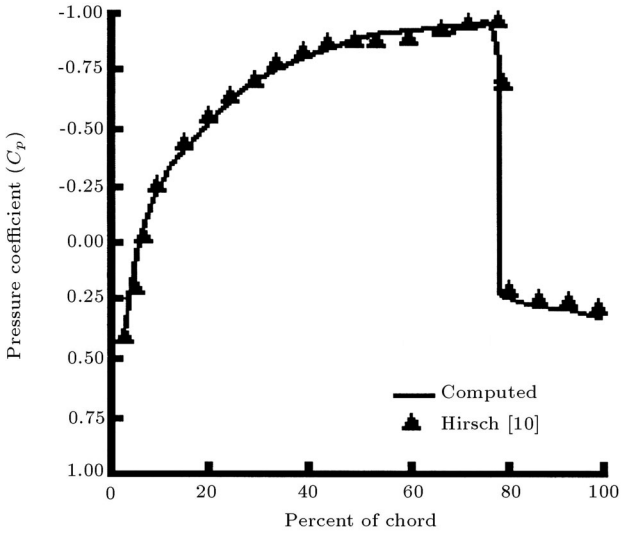

Figure 3. Comparing the computed and reference curves of pressure coefficient (Cp) for flow over a NACA0012 airfoil. The Mach number is 0.85 and the angle of attack is zero.

plate. This study gives an adequate assurance of the viscous solution of the solver with the implemented turbulence model. Additionally, the good agreement of the results with the experimental results reported by Bohn et al. [8] demonstrated in Figure 4, shows that the grid resolution 200×80 used for the computational domain, is sufficient to capture the boundary layer.

The third test study is prepared for the subsonic viscous flow over a NACA0012 airfoil. The Reynolds number is set to 10^6 and the flow is turbulent. The inlet Mach number is set to 0.4 and the angle of attack is set to zero. Figure 5 shows the computed results, which are in good agreement with experimental results reported by Fletcher [11]. This test case is prepared

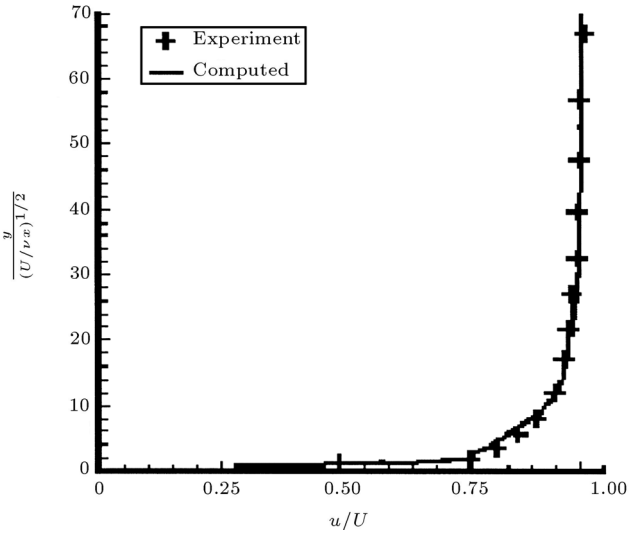

Figure 4. Comparing the computed velocity profile for flat plate with the experimental profile at 68% of the plate length, from the leading edge of the flat plate.

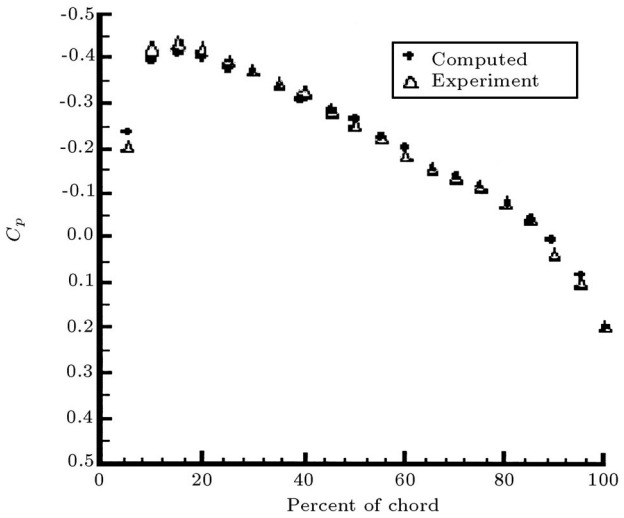

Figure 5. Computed and experimental pressure coefficients over a semi NACA0012 airfoil. Mach number is 0.4 and Reynolds number is 10^6.

to examine the solver in viscous-turbulent flows with the existence of pressure gradients. This condition is very usual in flows through axial compressor stages. The grid resolution is the same as that of flat plate problems.

Numerical Studies for a Compressor Stage

The test cases mentioned above give an adequate assurance for using the solver in computational studies, both in inviscid and viscous approaches. The two final studies are prepared for flow through a compressor stage at a stable point on the operating line of the compressor.

The parameters of the compressor operating condition are given in Table 2 and the geometrical characteristics of the stage are given in Table 3.

Figure 6 shows the stage as a multi-block (20 blocks) zone, where each block is the passage between the upper and lower blade of two adjacent blades in each row. The rotor and stator rows each contain 9 blades and, consequently, 10 passages.

Table 2. Operating condition parameters.

$\frac{r_h}{r_t}$	0.6
$\mathbf{R}$	0.56
$\boldsymbol{P}_{\text{in}}$	100000 Pa
$\boldsymbol{T}_{\text{in}}$	300 K°
$\boldsymbol{\beta_1}$	62°
$\boldsymbol{\psi}$	0.28
$\boldsymbol{\phi}$	0.4
$\boldsymbol{M}_{\text{in}}$	0.223
$\boldsymbol{U_r}$	90 m/s

Table 3. Geometrical characteristics of the stage.

Stagger angle of rotor blades	55°
Stagger angle of stator blades	35°
Rotor blade profile	NACA65-(A_{10})
Stator blade profile	NACA65-(A_{10})
Solidity	1.0
Gap in percent of chord	37%

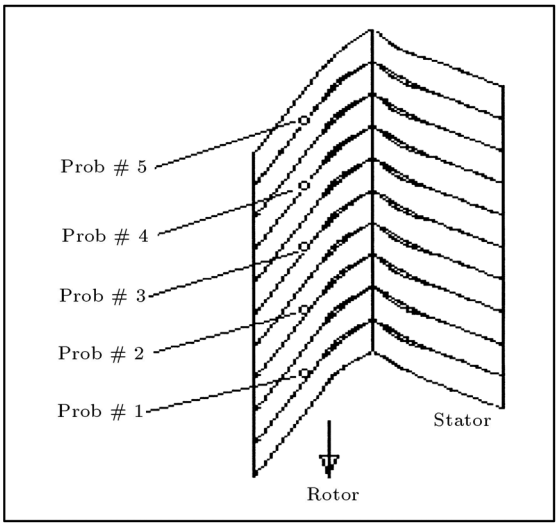

Figure 6. Multi-block geometry of the compressor stage.

The grid used in each passage is 75×41 with clustering and orthogonality near the solid walls. The total number of finite volume cells is 61500 for the computational domain of the stage. The mesh is used for both inviscid and viscous studies to prepare the uniformity on a grid basis for numerical comparison of the two approaches. To show the independency of the solution to the implemented grid resolution, a double-passage (four blocks) stage is studied with three grid resolutions; $151 \times 81, 75 \times 41$ and 45×21 for each block. Figure 7 shows the double-passage geometry which contains four blocks.

The convergence history of the three grid cases are shown in Figure 8. The history is based on a logarithm of the normalized error for the continuity equation evaluated over the entire computational area of the lower rotor block.

Figure 8 illustrates that the resolutions 151×81 and 75×41 have the same level of accuracy in the same solution cycles, whereas the resolution 45×21 does not provide the desired accuracy and, thus, cannot be adequate for the numerical study. As a result, for

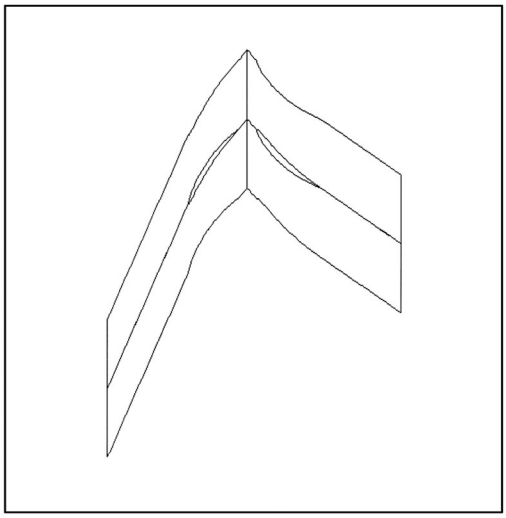

Figure 7. The double-passage stage geometry for the grid dependency study.

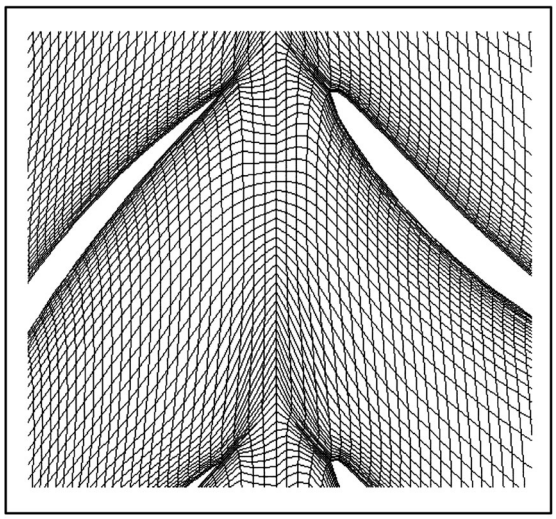

Figure 9. Partial illustration of mesh generated for the stage.

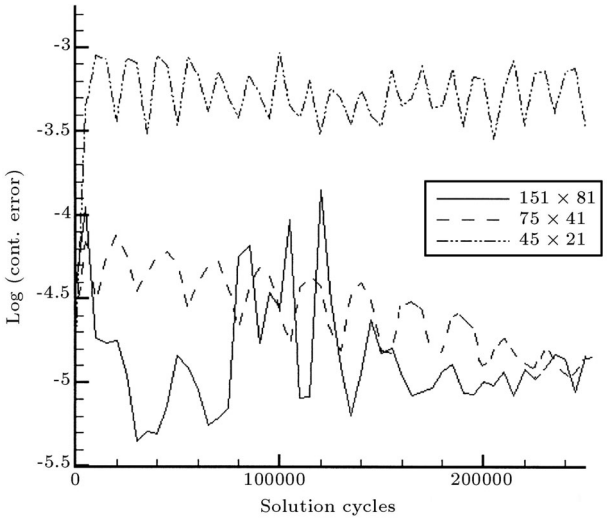

Figure 8. The convergence history of the three implemented grid resolutions $151 \times 81, 75 \times 41$ and 45×2, for the double-passage stage problem.

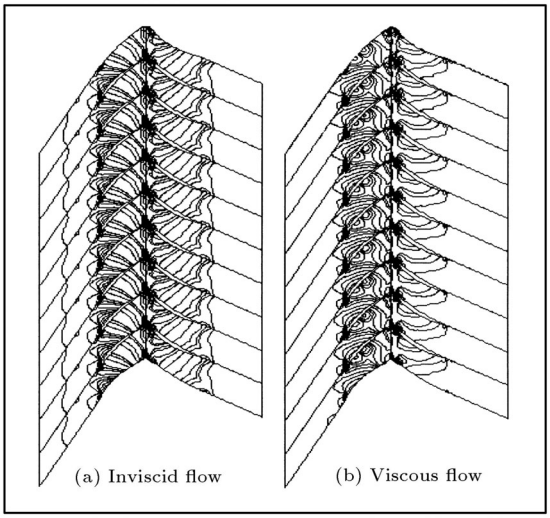

Figure 10. Pressure contours for inviscid and viscous approaches.

each block, the grid resolution 75×41 is used for the computational studies which follow.

Five probes are located near the leading edge of the blades in the rotor row, to indicate the required parameters. Figure 9 shows a zoomed area of the grid used in the stage problem. The clustering and near orthogonality near the solid surfaces are illustrated in this figure.

In Figure 10, the pressure contours of the inviscid and viscous solutions and, in Figure 11, the Mach contours of the inviscid and viscous solutions are shown, respectively. The streamlines obtained from inviscid and viscous solutions are also shown in Figure 12, respectively, in an absolute frame. Finally, the velocity vectors in an absolute frame (stationary frame), obtained from two different solutions, are also shown in Figures 13a and 13b. The results of Figures 10 to 13 are nearly similar but not exactly the same. To give a more detailed comparison of the two approaches, Table 4 is prepared, in which pressure, Mach number and axial velocity for inviscid and viscous solutions are compared with each other. In the final row of the table, the relative error of the inviscid solution is computed for each parameter, with respect to the viscous solution. The flow parameters in Table 4 are obtained from the probes shown in Figure 6.

CONCLUSION

A multi-block, 2-D solver was developed to investigate inviscid and viscous approaches in turbomachinery through-flow problems. Inviscid flow around an air-

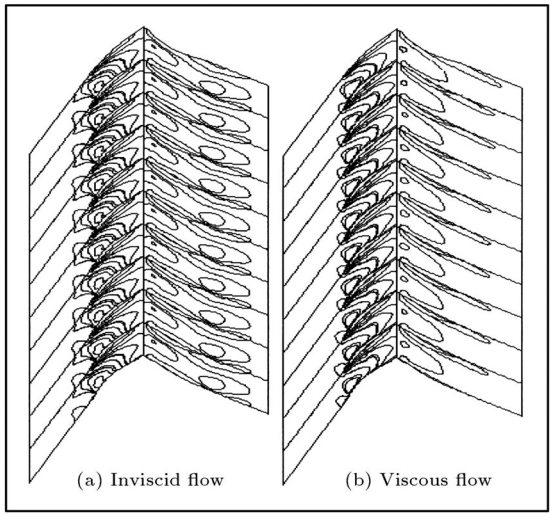

Figure 11. Mach contours for inviscid and viscous approaches.

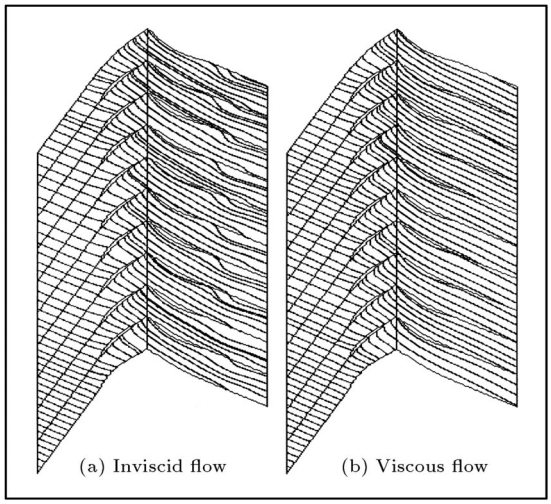

Figure 12. Streamlines in absolute frame.

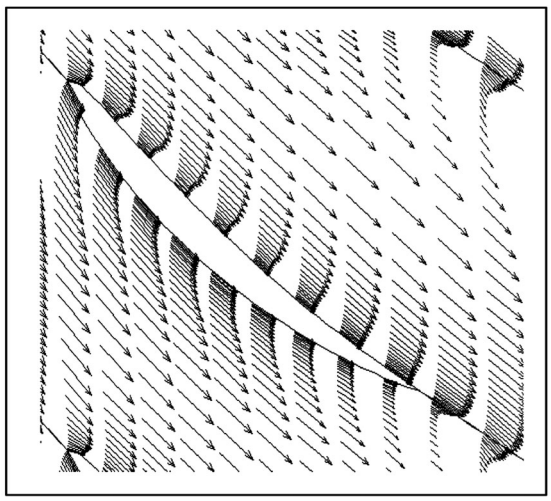

Figure 13a. Velocity vectors in absolute frame (inviscid solution).

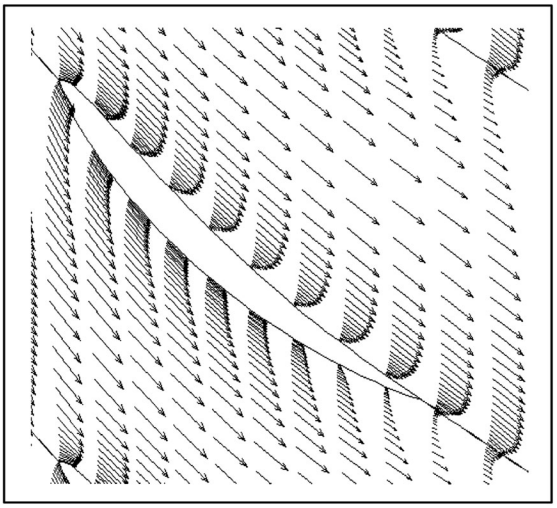

Figure 13b. Velocity vectors in absolute frame (viscous solution).

foil, NACA0012, was observed to show the required assurance of the solver in the inviscid part of the solution. Further, the viscous-turbulent flow over a flat plate and the NACA0012 airfoil were observed, in order to validate the solver and the grid resolution in viscous-turbulent flows. The test cases of NACA0012 airfoil gave the required assurance about the solver.

The inviscid and viscous flows are solved separately for a stage of an axial compressor with a specified geometry and at a stable operating condition. The results obtained from probes located in the computational domain and other results shown in Figures 9 to 12, show some differences between the results obtained from the inviscid and viscous approaches. The results show that the inviscid solution has a relative error of about 5 to 7 percent, which may cause more errors in computing the performance of the stage. However, the CPU time of the viscous solution was 30 percent greater than that of the inviscid solution. On the other hand, if the flow condition deviates from its stable operating condition, the deviated flow incidence angles may cause large separated areas in the stage and, as a result, the errors of an inviscid approach may exceed very large values.

As a final conclusion, with attention to the errors of the inviscid solution, including the unknown risks of using this approach in unstable conditions and with a 30% excess of CPU time for viscous solutions, it would appear to be more accurate and safe to use the viscous approach in turbomachinery numerical studies. However, it is also evident that for a rapid estimation of flow parameters, the inviscid approach can be used.

For future works, the flow in unstable and separated conditions can be investigated with both approaches, to prepare a more complete comparison of

Table 4. Comparison of flow parameters obtained from inviscid and viscous solutions.

Probe No.	**Pressure (Pa)**	
	Inviscid	**Viscous**
1	93900	100600
2	93900	100600
3	93900	100600
4	93900	100600
5	93900	100600
Relative Error (%)	6.7	
Probe No.	**Mach Number**	
	Inviscid	**Viscous**
1	0.234	0.221
2	0.234	0.221
3	0.234	0.221
4	0.234	0.221
5	0.234	0.221
Relative Error (%)	5.9	
Probe No.	**Axial Velocity (m/s)**	
	Inviscid	**Viscous**
1	39.6	37.00
2	39.6	37.00
3	39.6	37.00
4	39.6	37.00
5	39.6	37.00
Relative Error (%)	7.0	

inviscid and viscous approaches in off-design conditions.

NOMENCLATURE

τ	time in transformed coordinate time step
σ	stress tensor
ω	slope averaging parameter
ξ	horizontal axis of transformed coordinate
ρ	density
μ	absolute viscosity
β_1	inlet angle of relative velocity
ψ	load coefficient
ϕ	flow coefficient
η	vertical axis of transformed coordinate
$\hat{\delta}^+, \overline{\delta}^+$	limited slopes velocity of sound
E	total energy vector
$\overline{\mathbf{E}}_E$	inviscid transformed flux vector
$\overline{\mathbf{E}}_v$	viscous transformed flux vector
$\vec{\mathbf{F}}$	total flux tensor
$\vec{\mathbf{F}}_E$	inviscid flux tensor
$\vec{\mathbf{F}}_v$	viscous flux tensor
$\overline{\mathbf{F}}_E$	inviscid transformed flux vector
$\overline{\mathbf{F}}_v$	viscous transformed flux vector
H	total enthalpy
$\mathbf{I}$	unit tensor
i	cell index in ξ direction
i_{block}	block index
$i_{\max}$	maximum cell index in ξ direction
j	cell index in η direction
J	Jacobian of transformation
$j_{\max}$	maximum cell index in η direction
k	$k = \frac{C_p}{C_v}$
ℓ	limiter function
$\mathbf{M}$	Mach number
$\mathbf{M}_{\text{in}}$	inlet Mach number
$\mathbf{n}$	normal vector
P	thermodynamic pressure
P_{in}	inlet pressure
$\mathbf{q}$	heat flux
$\mathbf{Q}$	vector of conservative variables
$\overline{\mathbf{Q}}$	transformed vector of conservative variables
R	reaction factor
r	parameter of MUSCL limiter
r_h	hub radius
r_t	tip radius
t	time in physical coordinate
T_s	static temperature
T_{in}	inlet temperature
$\mathbf{u}$	velocity vector
u	x-direction velocity component
$\widetilde{u}$	averaged $\mathbf{u}$ at cell boundary
v	y-direction velocity component
V	volume
x	vertical axis of Cartesian coordinates
y	horizontal axis of Cartesian coordinate

Subscript

ξ	partial derivative with respect to ξ
η	partial derivative with respect to η

b	index of bottom face flux
h	hub for blade radius
E	inviscid flux vector
i	mesh point index in ξ direction
in	inlet condition
j	mesh point index in η direction
l	index of left face flux
r	index of right face flux
t	index of top face flux
t	tip for blade radius
t	total state for thermodynamic properties
x	partial derivative with respect to x
y	partial derivative with respect to y
v	viscous flux vector

Superscript

n	previous time level
$n+1$	current time level
T	transpose matrix

REFERENCES

1. Sisto, F., Wu, W., Thangam, S. and Jonnavithula, S. "Computational aerodynamics of oscillating cascade with evolution of rotating stall", *AIAA Journal*, **27**(4), pp 462-471 (1989).
2. Jonnavithula, S., Thangam, S. and Sisto, F. "Computational and experimental study of stall propagation in axial compressors", *AIAA Journal*, **28**(11), pp 1945-1952 (1990).
3. He, L. "Computational study of rotating-stall inception in axial compressors", *Journal of Propulsion and Power*, **13**(1), pp 31-38 (Jan.-Feb., 1997).
4. Outa, E., Kato, D. and Chiba, K. "AN N-S simulation of stall cell behavior in a 2-D compressor rotor-stator system at various load", *ASME Paper* (94-GT-257) (1994).
5. Saxer-Flelici, H.M., Saxer, A.P., Inderbitzen, A. and Gyarmathy, G. "Prediction and measurement of rotating stall cell in an axial compressor", *ASME Journal of Turbomachinery*, **121**, pp 365-375 (1999).
6. Hoffman, K.A. and Chiang, S.T., *Computational Fluid Dynamics for Engineers*, A Publication of Engineering Education System^{TM}, Wichita, Kansas, ISBN 0-9623731-7-6, USA (1993).
7. Peyret, R., Grasso, F. and Meola, C. "Handbook of computational fluid mechanics", *Euler and Navier-Stokes Equations for Compressible Flows: Finite Volume Methods, Academic Press*, Chapter 4, ISBN 0-12-553010 (1996).
8. Bohn, D. and Emunds, R. "A navier-stokes computer code for theoretical investigations on the application of various turbulence models for flow prediction along turbine blades", *Proceeding of the International Gas Turbine and Aero-Engine Congress and Exposition*, Houston, Texas-June 5-8, 95-GT-90 (1995).
9. Farhanieh, B. and Amanifard, N. "Numerical investigation on compressible flow characteristics in axial compressors using a multi-block finite-volume scheme", *International Journal of Engineering*, **15**(1), pp 91-104 (2002).
10. Hirsch, Ch. "Numerical computation of internal and external flows", *Fundamentals of Numerical Discretization*, A Wiley-Interscience Publication, **1**, ISBN 0 471 917621 (1988).
11. Fletcher, C.A.J., *Computational Techniques for Fluid Dynamics 2*, Springer-Verlag, ISBN 0-387-18759-6 (1991).